Level Set Segmentation of Brain Matter Using a Trans-Roto-Scale Invariant High Dimensional Feature

Naveen Madiraju[1], Amarjot Singh[2(✉)], and S.N. Omkar[3]

[1] Department of ECE, National Institute of Technology, Warangal, India
[2] Faculty of Applied Sciences, Simon Fraser University, Burnaby, Canada
asa168@sfu.ca
[3] Department of Aerospace Engineering, Indian Institute of Science, Bangalore, India

Abstract. Brain matter extraction from MR images is an essential, but tedious process performed manually by skillful medical professionals. Automation can be a potential solution to this complicated task. However, it is an ambitious task due to the irregular boundaries between the grey and white matter regions. The intensity inhomogeneity in the MR images further adds to the complexity of the problem. In this paper, we propose a high dimensional translation, rotation, and scale-invariant feature, further used by a variational framework to perform the desired segmentation. The proposed model is able to accurately segment out the brain matter. The above argument is supported by extensive experimentation and comparison with the state-of-the-art methods performed on several MRI scans taken from the McGill Brain Web.

1 Introduction

Accurate brain matter segmentation is essential for the study of various ailments such as multiple sclerosis [1], Alzheimer [2], and Parkinson disease [2]. Hence, skilled medical professionals spend a considerable amount of their time manually labeling white and grey matter in the MR images. However, accurate labeling of brain matter is a tedious process due to which substantial difference in labeling is observed for different labelers. This difference can potentially be avoided by making use of automatic methods that are capable of automatically segmenting the brain matter.

Automated segmentation of the brain matter from the MR images is a particularly challenging task. The brain matter varies considerably in shape and size with irregular boundaries making gradient-based algorithms inefficient. Moreover, the corruption of images with a smoothly varying intensity inhomogeneity caused due to the image acquisition defects [3] further hinders the segmentation process. In addition, both tissues (grey and white) can have similar intensity levels in certain regions that further adds to the complexity of the problem. The within-tissue intensities for both tissues can also vary greatly, making it impossible to classify images based on pixel intensities.

C.-S. Chen et al. (Eds.): ACCV 2016 Workshops, Part II, LNCS 10117, pp. 595–609, 2017.
DOI: 10.1007/978-3-319-54427-4_43

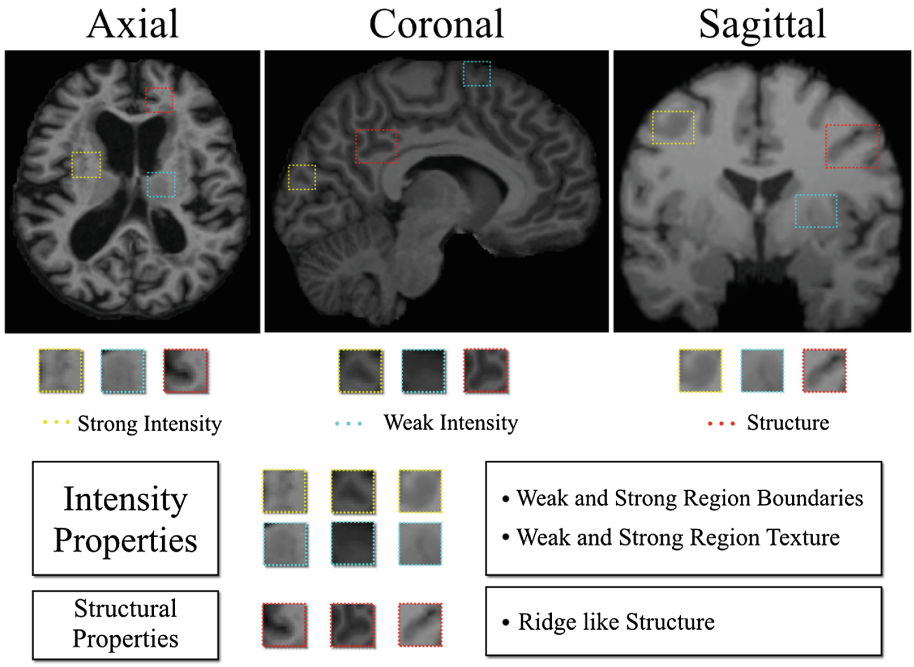

Fig. 1. Illustrates intensity and structural properties extracted from axial, coronal and sagittal view of brain MRI. It is shown that (weak, strong) region boundaries and texture are covered under intensity properties while ridge like structures are covered with structural properties.

In the recent past, numerous *two-stage* segmentation strategies have been recommended for brain matter segmentation [4–13]. Most of the strategies include a primary stage that extracts a high-dimensional feature, which combines the structural and intensity properties (as in Fig. 1) of brain matter in MR images. This high-dimensional feature is further used by a secondary supervised or a variational framework to achieve the desired brain matter segmentation. Supervised approaches use labeled data to automatically learn a model that is further used by a classifier such as Support vector machines [14], Markov random field [15], Neural networks [16] etc., for segmentation. However, statistical classification approaches are inefficient due to the presence of irregular boundaries and intensity inhomogeneity as mentioned above. On the contrary, variational methods have been relatively successful for medical image segmentation due to their ability to achieve sub-pixel accuracy and immunity towards topological changes [17,18]. These methods can also effectively coordinate distinctive information in a principled manner (e.g., boundary information, region information, shape priors, texture for vector valued images) [2,19,20] to achieve optimal segmentation by minimizing the energy function defined in level sets framework.

Multiple methods have been introduced that incorporate local intensity information in an energy framework for image segmentation [21–25]. However, local

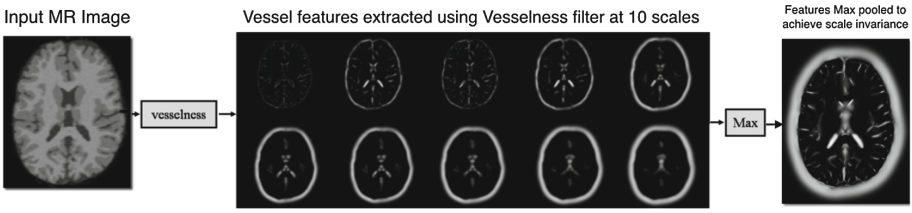

Fig. 2. Illustrates the vesselness feature extracted at 10 different scales. Next, max pooling is applied to achieve a scale invariant feature.

intensity itself may not be sufficient for accurate segmentation in the presence of heavy noise and intensity inhomogeneity [22]. Recently, Wang et al. [22] characterized an energy equation using local Gaussian distribution fitting of image intensities. This energy was minimized using level set to achieve the brain matter segmentation. He et al. [20] proposed a method that used local entropy feature derived from the grey level distribution of MR image instead of intensity, for segmentation. Further, Huang et al. [26] combined voxel probability, image gradient, and curvature information to achieve brain tissue segmentation. Finally, Popuria et al. [27] used various MRI modalities and their texture characteristics to construct a multi-dimensional feature set to achieve the same task.

The above-mentioned studies have proven that a combined feature set is well suited for brain matter segmentation as opposed to a single feature. However, no explanation is provided as to what kind of features best captures the properties of the brain matter in MR images. In this paper, a two-stage segmentation pipeline is used to achieve brain matter segmentation from MR images. The first stage of the pipeline uses a proposed translation, rotation and scale invariant high-dimensional feature derived by combining three sub-features that best represent the structural and intensity properties of the brain matter. The proposed high-dimensional feature is then used by a novel variational level sets method [28] to achieve the desired brain matter segmentation.

The main contributions of the first and second stage of the proposed segmentation pipeline are presented as below:

– *High-dimensional Feature*: The first stage of the architecture proposes a high dimensional feature that captures the intensity and structural properties of the brain matter. The intensity properties are represented in the brain matter by region boundaries and texture while the ridge-like structures correspond to the structural properties of the matter as shown in Fig. 1. Gabor [29] and Texture [30] filters were used to represent the intensity properties of the brain while the structural properties were extracted using a vesselness [31] filter. The intensity and structural properties can appear at any position, orientation and scale in the MR images. Hence, invariance to translation, rotation, and scale is introduced in each sub-feature. The invariant sub-features are weighted and

combined to derive the high dimensional feature that precisely represents the brain matter properties.
– *Variational Framework*: The second stage of the pipeline uses an extended version of the variational framework proposed by Li et al. [28]. The variational framework is adapted to accommodate the proposed high dimensional feature as the objective function obtained by integration over the whole image domain. The objective function is minimized in the level-set framework to achieve the desired brain matter segmentation.

The remaining of this paper is organized as follows. The next section presents the proposed two-stage architecture for brain matter segmentation. The first subsection describes the formulation of the high dimensional feature and the reasons for selecting the specific sub-features. The second subsection illustrates the formulation of the variational framework and the minimization of the objective function with the incorporated high dimensional feature. Finally, Sect. 3 details the experimental results along with a qualitative and quantitative comparison with the state of the art methods. Section 4 presents the conclusions.

2 Proposed Model

This section details the proposed two-stage brain matter segmentation pipeline. In the first sub-section, the sub-features chosen to formulate the proposed high-dimensional feature are presented. Next, the mathematical formulation that presents the incorporation of the proposed high-dimensional feature within the Li et al.'s variational framework is introduced. Finally, the detailed derivation for the minimization of the objective function with the incorporated high-dimensional feature, that results in the desired brain matter segmentation, is presented.

2.1 Proposed High-Dimensional Feature

The proposed High-Dimensional feature is composed of three sub-features that attempt to capture the structural and intensity properties of the brain matter. Vesselness filter [31] is used to capture the ridge-like structural features of the brain matter while the intensity properties in the form of region boundaries and texture are captured using Gabor [32] and MR8 [33] texture filters respectively. The structural and intensity properties are shown in Fig. 1.

1. *Vesselness:* The brain matter contains ridge structures that can be exploited for superior segmentation. A few articles in the recent past have presented systems for vessel or ridge extraction using the eigen-decomposition of the Hessian calculated at every pixel [31,34–38]. Further, Sofka et al. [31] developed an improvised filter to detect low contrast and narrow vessel structures. In this paper, the vessels are obtained by searching for tubular geometrical structures using second-order derivative information (principal curvatures of

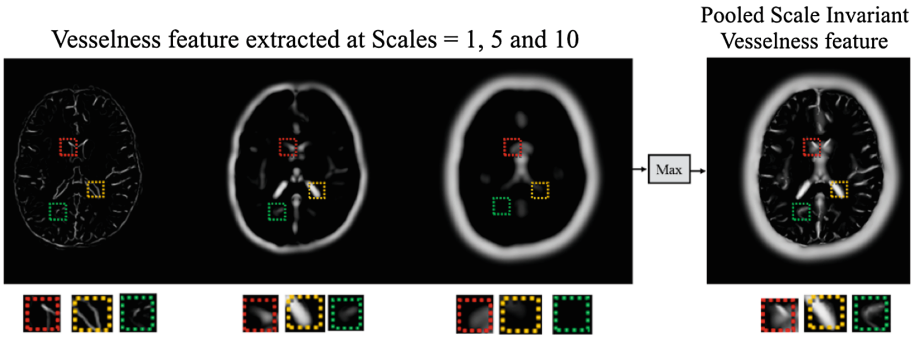

Fig. 3. Illustrates the max pooling of vesselness features at 3 different scales to achieve scale invariance. A 20×20 patch is selected at a spatial location from each feature map extracted at each scale. Max operation applied to the selected patches to achieve scale invariance.

image intensities). Vessels are distinguished by a locally prominent low curvature orientation (the vessel direction) and a plane of high-intensity curvature (the cross-sectional plane). The vesselness filter [31] uses the Hessian matrix to capture the above-mentioned geometric information. The local second-order structure of the image is decomposed into principal directions extracted using eigenvalue analysis of the Hessian. The eigenvalue decomposition extracts three orthonormal directions.

Invariance to scale is realized by extracting the vesselness using filters at different scales s, followed by the integration of their responses using a max operator to obtain a final estimate of vesselness as illustrated in Fig. 2. The process using which invariance is achieved is presented in detail in Fig. 3. A 10×10 patch is selected at a spatial location from each feature image extracted at every scale. A max operation is performed across patches selected from features extracted at each scales to achieve invariance as shown in Fig. 3. The process is detailed for 10 different scales due to lack of space.

2. *Edges*: The region boundaries separating the grey and white matter are important descriptors needed to distinguish between both matters. These descriptors can be extracted using edge detecting algorithms [32,39] developed in recent past. In this paper, one such method popularly known as Gabor filter is used to achieve rotation and scale invariance. Gabor [32] is a linear filter which is used to identify edges and line endings of white and grey matter over different scales and orientations. It's impulse response is determined by multiplication of harmonic function and gaussian function. Here, scale and rotational invariance are realized by extracting the Gabor features using filters at 3 scales and 8 orientation (as explained in the previous section), followed by the integration of their responses using a max operator to obtain rotation and scale invariance.

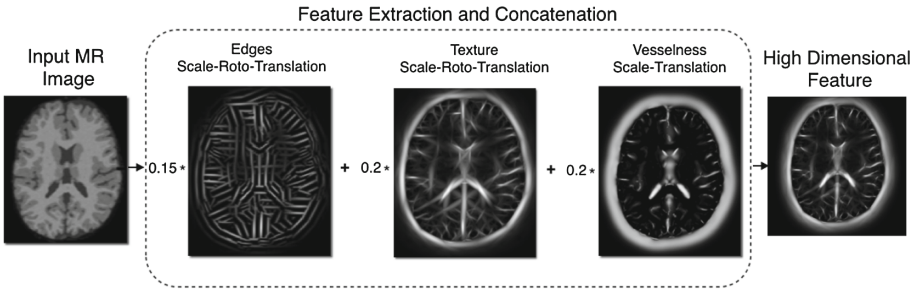

Fig. 4. Shows the weighted concatenation of all three invariant, gabor, texture and vessel feature to result into a trans-roto-scale high dimensional feature.

3. *Texture*: Texture is an another intensity property which can provide important information which can help to achieve optimal brain matter segmentation. It can be observed from the MR images that the grey matter has a more rough texture as compared to the white matter. The texture of an image is related to the spatial distribution of the intensity values of brain and white matter, and as such contains information regarding contrast, uniformity, rugosity, regularity, etc. This feature is efficient due to its sparse nature as it lies in lower dimensional subspaces. A few algorithms [33,40,41] were developed to extract this property. However, we make use of MR8 filter [33] to achieve roto-scale invariance. The texture information is captured using a MR8 filter bank [33] that consists of a Gaussian and a Laplacian of Gaussian (these filters have rotational symmetry) filter, an edge filter at 3 scales and a bar filter at the same 3 scales. The latter two filters are oriented and occur at 6 orientations at each scale. Measuring only the maximum response across orientations reduces the number of responses from 38 (6 orientations at 3 scales for 2 oriented filters, plus 2 isotropic) to 8 (3 scales for 2 filters, plus 2 isotropic) and achieves rotation invariance. A max operation is performed across the rotational invariant filters at different scales to achieve scale invariance in addition to rotation invariant to result into a roto-scale (rotation and scale) invariant feature (as explained above).

Features extracted at different scales and orientations using texture, edge, and vesselness filters are max pooled to achieve translational, rotational and scale invariance. The Fig. 2 shows vesselness features at 3 different scales, combined to achieve scale invariance. Similarly, Gabor based edges features and texture features at different scales and orientations are combined to achieve translational and rotational invariance. The invariant features are weighed and combined to give rise to a unified super feature that combines vesselness, edges and a texture filter features to derive a trans-roto-scale invariant high dimensional feature that is best suited for brain matter detection. The high dimensional feature is formulated by combining the above-mentioned sub features as presented below:

$$\mathcal{F} = \mathcal{V}_w \mathcal{V} + \mathcal{G}_w \mathcal{G} + \mathcal{T}_w \mathcal{T} \tag{1}$$

where $\mathcal{V}$ is vesselness feature, $\mathcal{G}$ is gabor feature and $\mathcal{T}$ is local texture feature while $\mathcal{V}_w$, $\mathcal{G}_w$ and $\mathcal{T}_w$ are the respective weights for each feature that decide the relative contribution of each feature. The similarity of the high dimensional feature with brain matter allows for better segmentation by the second stage of the architecture. The combined high dimensional feature is shown in Fig. 4.

2.2 Objective Function Formulation

In this section, the proposed high dimensional invariant feature is introduced in the variational segmentation framework proposed by [28] to achieve the brain matter segmentation. In this model, the MR image with the intensity inhomogeneity is formulated as:

$$I = bJ + n \tag{2}$$

Here I is the input image, b is the bias field which represents the amount of intensity inhomogeneity, n is the additive noise and J is the true image. In this model: (i) In a circular neighbourhood O_y centered at y the bias field is assumed to be constant (ii) Intensity belonging to the i^{th} tissue in a small circular neighbourhood should take a specific value c_i as in [19]. Here Neighbourhood size of O_y is controlled by a truncated gaussian kernel $K(y-x)$ defined by:

$$K(z) = \begin{cases} \frac{1}{a} e^{-|z|^2/2\sigma^2} & |z| \leq r, \\ 0 & \text{otherwise} \end{cases}$$

Here a is the normalization constant such that $\int K(z) = 1$. σ represents the size of the neighbourhood. We choose an optimal σ based on the level of intensity inhomogeneity of image.

The aim is to segment the image domain $\Omega \subset \mathcal{R}^2$ into three distinct regions namely: grey matter (Ω_1), white matter (Ω_2) and background (Ω_3). In order to achieve this task, a n-dimensional feature $\mathcal{F} : \{F_i ...\} \mid i \in \{1, 2..n\}$ with $\mathcal{F} \in \Omega$ is extracted from the input image I. Next, each circular neighbourhood region O_y is initially segmented into N (N=3) clusters using a localised K-means clustering. All the segmented circular neighbourhoods are integrated over the image domain Ω to obtain the energy functional given by:

$$\mathcal{E}_y = \int_\Omega \left(\sum_{i=1}^{3} \int_{\Omega_i} K(y-x) |\mathcal{F}(y)\,(I(x) - b(y)c_i)|^2 dx \right) dy \tag{3}$$

The label assigned to each subregion within a circular neighbourhood may or may not be true. In order to determine the most probable label for each region, the energy functional is minimised as described in the next section.

2.3 Objective Function Minimization in Level-Set Framework

The energy equation is minimised by modifying the proposed energy functional equation as mentioned in the previous section into the level sets framework. In

order to segment the image in N=3 disjoint regions, atleast two ($n > log(N)$) level set functions $\Phi = (\phi_1, \phi_2)$ are required [25]. The energy functional equation is modified using the membership function M_i for each disjoint region as below:

$$\mathcal{E}(\phi, c_i, b) = \sum_{i=1}^{3} \int_{\Omega} \left(\int_{\Omega} K(y-x)\mathcal{F}^2(y)|I(x) - b(y)c_i|^2 M_i(\phi(x))dy \right) dx \quad (4)$$

Here $ci = (c_1, c_2, c_3)$ and $M_i = (M_1, M_2, M_3)$. For simplicity, we use vector forms for $\mathbf{c} = (c_1, c_2, c_3)$ and $\mathbf{\Phi}(\mathbf{x}) = (\phi(x)_1, \phi(x)_2, \phi(x)_3)$. Equation 4 can be further simplified as below:

$$\mathcal{E}(\mathbf{\Phi}, \mathbf{c}, b) = \sum_{i=1}^{3} \int_{\Omega} (e_i(x) M_i(\mathbf{\Phi}(\mathbf{x}))dx) \quad (5)$$

where $e_i(x) = \int_{\Omega} K(y-x)\mathcal{F}^2(y)|I(x) - b(y)c_i|^2)dy$. For mathematical simplification we expand integral and rewrite e_i as

$$e_i(x) = I^2(x)T_1 - 2c_i I(x)T_2 + c_i^2 T_3 \quad (6)$$

where $T_1 = \int_{\Omega} K(y-x)\mathcal{F}^2(y)dy$, $T_2 = \int_{\Omega} K(y-x)\mathcal{F}^2(y)b(y)dy$ and $T_3 = \int_{\Omega} K(y-x)\mathcal{F}^2(y)b^2(y)dy$.

In order for the level set to effectively segment the image into the required disjoint regions, the energy functional is formulated using two regularization terms, $\mathcal{L}(\phi_j)$ and $\mathcal{R}(\phi_j)$, where j is the number of level set functions. The entire energy functional with regularization terms is mentioned below:

$$E(\mathbf{\Phi}, \mathbf{c}, b) = \mathcal{E}(\mathbf{\Phi}, \mathbf{c}, b) + \nu \left(\sum_{j=1}^{2} \mathcal{L}(\phi_j) \right) + \mu \left(\sum_{j=1}^{2} \mathcal{R}(\phi_j) \right) \quad (7)$$

where $\mathcal{L}(\phi)$ and $\mathcal{R}(\phi)$ are defined as in [42] as follows:

$$\mathcal{L}(\phi) = \int |\nabla H(\phi(x))|dx \quad (8)$$

$$\mathcal{R}(\phi) = \int \frac{1}{2} \left(|\nabla \phi(x)| - 1 \right)^2 dx \quad (9)$$

where H is the heaviside function. The membership function can also be written using the heaviside function as: $M_1(\phi_1, \phi_2) = H(\phi_1)H(\phi_2)$, $M_2(\phi_1, \phi_2) = H(\phi_1)\left(1 - H(\phi_2)\right)$ and $M_3(\phi_1, \phi_2) = 1 - H(\phi_1)$. The heaviside function H can be approximated by a smooth function H_ϵ defined by

$$H_\epsilon(u) = \frac{1}{2} \left[1 + \frac{2}{\pi} arctan\left(\frac{u}{\epsilon} \right) \right] \quad (10)$$

The derivative of H_ϵ is given by

$$\begin{aligned} \delta_\epsilon(u) &= H'_\epsilon(u) \\ &= \frac{1}{\pi} \frac{\epsilon}{\epsilon^2 + u^2} \end{aligned} \quad (11)$$

The entire energy functional Eq. 7 is minimized with respect to $\mathbf{\Phi}$ to achieve optimal image segmentation. The energy is minimized through the following gradient flow equations:

$$\begin{aligned}\frac{\partial \phi_1}{\partial t} =& -\delta(\phi_1)\left(H(\phi_2)e_1 + (1-H(\phi_2))\,e_2 - e_3\right) \\ &+ \nu\delta_\epsilon(\phi_1)div\left(\frac{\nabla\phi_1}{|\nabla\phi_1|}\right) + \mu\left(\nabla^2\phi_1 - div\left(\frac{\nabla\phi_1}{|\nabla\phi_1|}\right)\right)\end{aligned} \tag{12}$$

$$\begin{aligned}\frac{\partial \phi_2}{\partial t} =& -\delta(\phi_2)\left(H(\phi_1)e_1 - H(\phi_1)e_2\right) \\ &+ \nu\delta_\epsilon(\phi_2)div\left(\frac{\nabla\phi_2}{|\nabla\phi_2|}\right) + \mu\left(\nabla^2\phi_2 - div\left(\frac{\nabla\phi_2}{|\nabla\phi_2|}\right)\right)\end{aligned} \tag{13}$$

To find optimal $\mathbf{c}$, we keep $\mathbf{\Phi}$ and b constant and minimize the energy equation with respect to $\mathbf{c}$. The optimal $\mathbf{c}$ is given by:

$$c_i = \frac{\int_\Omega \left(\left(\mathcal{F}^2 b\right) * K\right) I(x) M_i(\mathbf{\Phi}(x))dx}{\int_\Omega \left(\left(\mathcal{F}^2 b^2\right) * K\right) I(x) M_i(\mathbf{\Phi}(x))dx} \tag{14}$$

Similarly by making $\mathbf{\Phi}$ and $\mathbf{c}$ constant, we minimize the energy equation with respect to b. This can be written as:

$$b(y) = \frac{(S_1 I) * K}{(S_2 I) * K} \tag{15}$$

where $S_1 = \sum_{i=1}^{3} c_i M_i(\mathbf{\Phi}(x))$ and $S_2 = \sum_{i=1}^{3} c_i^2 M_i(\mathbf{\Phi}(x))$.

3 Experimentation

In this section, the parameter setting of the high-dimensional feature along with the experimentation details of the proposed algorithm is presented in detail. The parameters of the high dimensional feature are tuned on 60 brain MRI images chosen from the McGill Brain Web [43]. The performance of the proposed algorithm using the optimal high-dimensional feature is evaluated using the quantitative and qualitative results on 40 brain MR images. In addition, the qualitative and quantitative comparison are presented with 3 state-of-the-art brain segmentation methods. In addition, the quantitative comparison is further extended to 10 addition brain segmentation methods. The comparison is presented at different levels of intensity non-uniformity (INU) and noise in the subsequent sections.

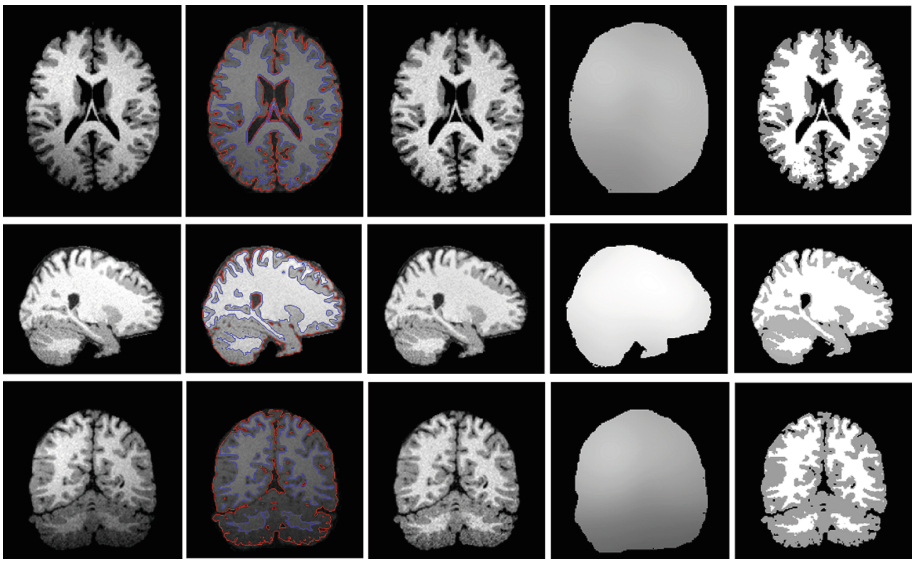

Fig. 5. Application of proposed method to axial, coronal and sagittal slices of brain MR images. Column 1: original images. Column 2: final contours. Column 3: corrected image. Column 4: bias field. Column 5: segmented image.

Parameters Setting: The parameters of the proposed method are set according to the attributes of the input images. In the subsequent discussion, the reasoning and values of the chosen parameters are provided. In the following experiments, all the parameters have values as follows:

1. We obtained the values of $\mathcal{V}_w$, $\mathcal{G}_w$ and $\mathcal{T}_w$ as 0.2, 0.15 and 0.2 respectively. The best feature weights ($\mathcal{V}_w$, $\mathcal{G}_w$, $\mathcal{T}_w$) for each feature are obtained heuristically using 60 training images. The process is discussed below: First, the weights for each feature (gabor, texture, and vessel) are randomly assigned using which the high dimensional feature is computed. This high dimensional feature is used in the objective function to obtain the cost value. The weights are modified after which the above-mentioned steps are repeated. The weights that result into the lowest cost value are finally decided that are used to form the final high dimensional feature.
2. As discussed by [28], a gaussian kernel of window size $64 * 64$ with a standard deviation $\sigma = 16$ is used to deal with high bias present in the Brain MRI.
3. The energy regularization coefficient μ and distance regularization coefficient ν are set as 1 and $0.001 * 255^2$ respectively as in [28]. The parameter ϵ in Heaviside function is set to 1 as discussed in chan and vese model [44].

Qualitative and Quantitative Results: Figure 5 shows the qualitative results obtained after applying the proposed algorithm to few images selected from the McGill Brain Web. The first column shows brain images of intensity non-uniformity(INU) = 100% and noise level of 3%. The second column shows final

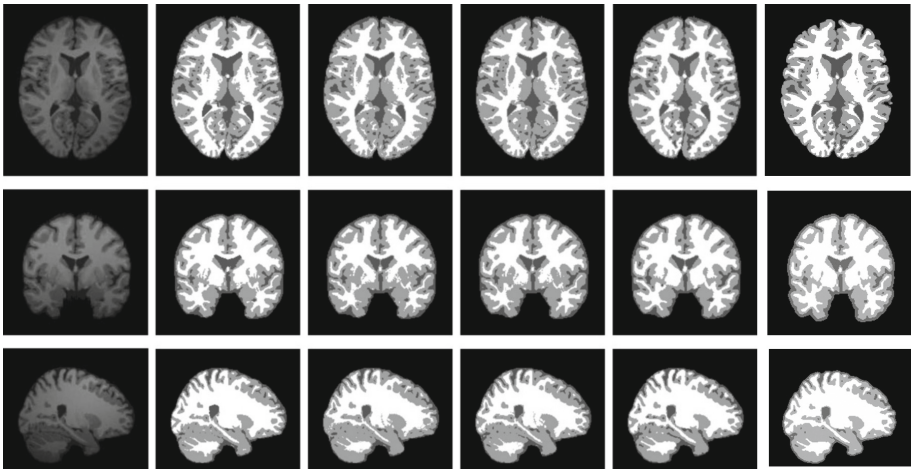

Fig. 6. Qualitative Comparison with Well et al.'s method [45], Leemput et al.'s method [1] and Wang et al.'s method [22] using simulated data obtained from McGill Brain Web. Column 1: original images. Column 2: Wells method. Column 3: Leemput's method. Column 4: Wang's method. Column 5: our proposed methodQualitative Comparison with Well et al.'s method [45], Leemput et al.'s method [1] and Wang et al.'s method [22] using simulated data obtained from McGill Brain Web. Column 1: original images. Column 2: Wells method. Column 3: Leemput's method. Column 4: Wang's method. Column 5: our proposed method

contour position while the third column shows the bias corrected images. The fourth column shows estimated bias field and the fifth column shows the segmented image. It can be observed that the intensities become sufficiently homogeneous within each tissue in the bias corrected images in column 3.

Next, Fig. 6 portrays the qualitative comparison of the proposed algorithm with the other state of the art methods. By careful observation of the segmentation results, as shown in Fig. 6, it can be inferred that our algorithm produces superior white matter segmentation results. For instance in Fig. 6, the lower left region of the sagittal image and in the lower region of the coronal image, the segmentation results of our algorithm looks most similar to ground truth. However, the segmentation results of other algorithms look similar to each other but are different from the ground truth. Further, we quantify the results and obtain that our algorithm yields more accurate results.

It is important to perform a quantitative evaluation in addition to the qualitative analysis to better understand the performance of the proposed method. In this paper, Jaccard similarity [3] measure is used to measure the similarity of the segmented regions with the ground truth. The measure is given by:

$$\mathcal{J}(S_1, S_2) = \frac{|S_1 \cap S_2|}{|S_1 \cup S_2|} \tag{16}$$

value of $\mathcal{J}$ lies between 0 and 1. Higher the value of $\mathcal{J}$ accurate the segmentation.

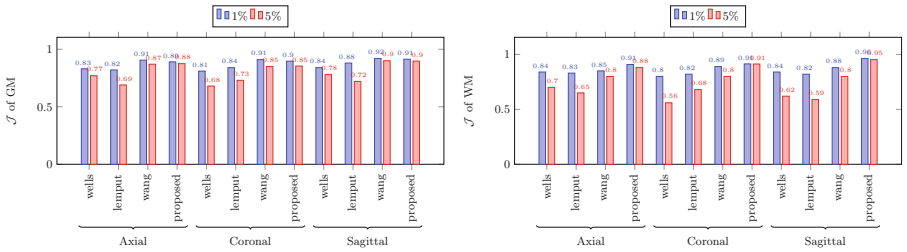

(a) Comparison of J similarity of Grey Matter segmentation results for various algorithms

(b) Comparison of J similarity of White Matter segmentation results for various algorithms

Fig. 7. Quantitative ($\mathcal{J}$) value comparison of algorithms for the 40 test images. The bar chart shows results of [1,22,45] and the proposed method applied on axial, coronal and sagittal slices of brain MR image at 1% and 5% noise levels.

A bar graph is shown in Fig. 7 portrays a Jaccard similarity $\mathcal{J}$ comparison of segmentation results for both grey and white matter for the proposed and state of the methods. From Fig. 7(a) shows grey matter segmentation results at 1% noise levels. It can be observed that our algorithm produces slightly poor results as compared to Wang et al.'s method [22] but yields superior results compared to Well et al.'s method [45] and Leemput et al.'s method [1]. However, in presence of 5% noise, our algorithm performs better than rest of the algorithms.

Table 1. The table shows comparison of average Jaccard ($\mathcal{J}$) values of grey matter and white matter of our algorithm with current state of the art algorithms.

Method	$\mathcal{J}$ of grey matter	$\mathcal{J}$ of white matter
Adaptive MAP [6]	0.564	0.567
Biased MAP [6]	0.558	0.562
Fuzzy c-means [6]	0.473	0.567
Maximum-a-posteriori (MAP) [6]	0.550	0.554
Maximum-likelihood [6]	0.535	0.551
Tree-structure k-means [6]	0.477	0.571
MPM-MAP [7]	0.662	0.683
BSE/BFC/PVC [8]	0.595	0.664
Constrained GMM (MAP) [9]	0.680	0.660
Spatial-varying GMM [10]	0.768	0.734
Coupled surface [11]	0.701	NA
FSL [12]	0.756[2]	NA
SPM [13]	0.790[2]	NA
MAP with histograms [6]	0.814	0.710
Decision forest classifier [12]	0.838	0.731
Our algorithm	**0.89**	**0.91**

Subsequently, Fig. 7(b) shows white matter segmentation results. It can be perceived that our algorithm performs better at both 1% and 5% noise setting than other methods. It can be concluded that our algorithm produces superior results in presence of high bias and high noise.

A more extensive comparison with other brain matter segmentation algorithms is presented in Table 1. The proposed algorithm outperforms the algorithms by a decent margin.

4 Conclusion

In this paper, we proposed a novel translation, rotation and scale invariant high dimensional feature that resembles the properties of brain matter. This proposed feature is used by level set based segmentation method to achieve sub-pixel segmentation of brain matter in the presence of noise and inhomogeneities. It is observed from the experiments that the high-dimensional feature gives superior segmentation performance over simple features. In addition, it can be concluded from the results that the similarity of the proposed feature to the structural and intensity properties of the brain matter further enhances the segmentation performance. Experiments demonstrate the superior performance of the proposed algorithm when compared to the state of the art methods.

References

1. Van Leemput, K., Maes, F., Vandermeulen, D., Suetens, P.: Automated model-based bias field correction of MR images of the brain. IEEE Trans. Med. Imaging **18**, 885–896 (1999)
2. Wang, L., Chen, Y., Pan, X., Hong, X., Xia, D.: Level set segmentation of brain magnetic resonance images based on local Gaussian distribution fitting energy. IEEE Trans. Med. Imaging **188**, 316–325 (2010)
3. Vovk, U., Pernus, F., Likar, B.: A review of methods for correction of intensity inhomogeneity in MRI. IEEE Trans. Med. Imaging **26**, 405–421 (2007)
4. Angoth, V., Dwith, C., Singh, A.: A novel wavelet based image fusion for brain tumor detection. IEEE Trans. Med. Imaging **2**, 1–7 (2013)
5. Dwith, C., Angoth, V., Singh, A.: Wavelet based image fusion for detection of brain tumor. IEEE Trans. Med. Imaging **5**, 25 (2013)
6. Yi, Z., Criminisi, A., Shotton, J., Blake, A.: Discriminative, semantic segmentation of brain tissue in MR images. In: Yang, G.-Z., Hawkes, D., Rueckert, D., Noble, A., Taylor, C. (eds.) MICCAI 2009. LNCS, vol. 5762, pp. 558–565. Springer, Heidelberg (2009). doi:10.1007/978-3-642-04271-3_68
7. Marroquín, J.L., Vemuri, B.C., Botello, S., Calderón, F., Fernandez-Bouzas, A.: An accurate and efficient Bayesian method for automatic segmentation of brain MRI. IEEE Trans. Med. Imaging **21**, 934–945 (2002)
8. Shattuck, D.W., Sandor-Leahy, S.R., Schaper, K.A., Rottenberg, D.A., Leahy, R.M.: Magnetic resonance image tissue classification using a partial volume model. IEEE Trans. Med. Imaging **13**, 856–876 (2001)
9. Greenspan, H., Ruf, A., Goldberger, J.: Constrained Gaussian mixture model framework for automatic segmentation of MR brain images. IEEE Trans. Med. Imaging **25**, 1233–1245 (2006)

10. Peng, Z., Wee, W., Lee, J.H.: Automatic segmentation of MR brain images using spatial-varying Gaussian mixture and Markov random field approach. In: Conference on Computer Vision and Pattern Recognition Workshop, CVPRW 2006, pp. 80–80. IEEE (2006)
11. Zeng, X., Staib, L.H., Schultz, R.T., Duncan, J.S.: Volumetric layer segmentation using coupled surfaces propagation. In: Proceedings of 1998 IEEE Computer Society Conference on Computer Vision and Pattern Recognition, pp. 708–715. IEEE (1998)
12. Zhang, Y., Brady, M., Smith, S.: Segmentation of brain MR images through a hidden Markov random field model and the expectation-maximization algorithm. IEEE Trans. Med. Imaging **20**, 45–57 (2001)
13. Ashburner, J., Friston, K.: Multimodal image coregistration and partitioning–a unified framework. Neuroimage **6**, 209–217 (1997)
14. Magnin, B., Mesrob, L., Kinkingnéhun, S., Pélégrini-Issac, M., Colliot, O., Sarazin, M., Dubois, B., Lehéricy, S., Benali, H.: Support vector machine-based classification of Alzheimers disease from whole-brain anatomical MRI. Neuroradiology **51**, 73–83 (2009)
15. Khayati, R., Vafadust, M., Towhidkhah, F., Nabavi, M.: Fully automatic segmentation of multiple sclerosis lesions in brain MR flair images using adaptive mixtures method and Markov random field model. IEEE Trans. Med. Imaging **38**, 379–390 (2008)
16. Shen, S., Sandham, W., Granat, M., Sterr, A.: MRI fuzzy segmentation of brain tissue using neighborhood attraction with neural-network optimization. IEEE Trans. Med. Imaging **9**, 459–467 (2005)
17. Cobzas, D., Birkbeck, N., Schmidt, M., Jagersand, M., Murtha, A.: 3D variational brain tumor segmentation using a high dimensional feature set. In: IEEE 11th International Conference on Computer Vision, ICCV 2007, pp. 1–8. IEEE (2007)
18. Singh, A., Karanam, S., Bajpai, S., Choubey, A., Raviteja, T.: Malignant brain tumor detection. Int. J. Comput. Theor. Eng. **4**, 1002–1006 (2011)
19. Cui, W., Wang, Y., Lei, T., Fan, Y., Feng, Y.: Level set segmentation of medical images based on local region statistics and maximum a posteriori probability. Comput. Math. Methods Med. **2013**, 1–12 (2013)
20. He, C., Wang, Y., Chen, Q.: Active contours driven by weighted region-scalable fitting energy based on local entropy. IEEE Trans. Med. Imaging **92**, 587–600 (2012)
21. Li, C., Kao, C.Y., Gore, J.C., Ding, Z.: Minimization of region-scalable fitting energy for image segmentation. IEEE Trans. Med. Imaging **17**, 1940–1949 (2008)
22. Wang, L., He, L., Mishra, A., Li, C.: Active contours driven by local Gaussian distribution fitting energy. IEEE Trans. Med. Imaging **89**, 2435–2447 (2009)
23. Wang, Y., Xiang, S., Pan, C., Wang, L., Meng, G.: Level set evolution with locally linear classification for image segmentation. IEEE Trans. Med. Imaging **46**, 1734–1746 (2013)
24. Hahn, J., Lee, C.O.: Geometric attraction-driven flow for image segmentation and boundary detection. IEEE Trans. Med. Imaging **21**, 56–66 (2010)
25. Vese, L.A., Chan, T.F.: A multiphase level set framework for image segmentation using the Mumford and Shah model. IEEE Trans. Med. Imaging **50**, 271–293 (2002)
26. Albert, H., Rafeef, A., Roger, T., Anthony, T.: Automatic MRI brain tissue segmentation using a hybrid statistical and geometric model. In: 3rd IEEE International Symposium on Biomedical Imaging: Nano to Macro, pp. 394–397 (2006)

27. Karteek, P., Dana, C., Martin, J., Sirish L., S., Albert, M.: 3D variational brain tumor segmentation on a clustered feature set. In: Medical Imaging (2009)
28. Li, C., Huang, R., Ding, Z., Gatenby, J., Metaxas, D.N., Gore, J.C.: A level set method for image segmentation in the presence of intensity inhomogeneities with application to MRI. IEEE Trans. Med. Imaging **20**, 2007–2016 (2011)
29. Zacharaki, E.I., Wang, S., Chawla, S., Soo Yoo, D., Wolf, R., Melhem, E.R., Davatzikos, C.: Classification of brain tumor type and grade using MRI texture and shape in a machine learning scheme. IEEE Trans. Med. Imaging **62**, 1609–1618 (2009)
30. Pitiot, A., Delingette, H., Thompson, P.M., Ayache, N.: Expert knowledge-guided segmentation system for brain MRI. IEEE Trans. Med. Imaging **23**, S85–S96 (2004)
31. Frangi, A.F., Niessen, W.J., Vincken, K.L., Viergever, M.A.: Multiscale vessel enhancement filtering. In: Wells, W.M., Colchester, A., Delp, S. (eds.) MICCAI 1998. LNCS, vol. 1496, pp. 130–137. Springer, Heidelberg (1998). doi:10.1007/BFb0056195
32. Mehrotra, R., Namuduri, K.R., Ranganathan, N.: Gabor filter-based edge detection. IEEE Trans. Med. Imaging **25**, 1479–1494 (1992)
33. Geusebroek, J.M., Smeulders, A.W., Van de Weijer, J.: Fast anisotropic gauss filtering. IEEE Trans. Med. Imaging **12**, 938–943 (2003)
34. Aylward, S.R., Bullitt, E.: Initialization, noise, singularities, and scale in height ridge traversal for tubular object centerline extraction. IEEE Trans. Med. Imaging **21**, 61–75 (2002)
35. Lindeberg, T.: Edge detection and ridge detection with automatic scale selection. IEEE Trans. Med. Imaging **30**, 117–156 (1998)
36. Damon, J.: Properties of ridges and cores for two-dimensional images. IEEE Trans. Med. Imaging **10**, 163–174 (1999)
37. Lindeberg, T.: Feature detection with automatic scale selection. IEEE Trans. Med. Imaging **30**, 79–116 (1998)
38. Sato, Y., Nakajima, S., Atsumi, H., Koller, T., Gerig, G., Yoshida, S., Kikinis, R.: 3D multi-scale line filter for segmentation and visualization of curvilinear structures in medical images. In: Troccaz, J., Grimson, E., Mösges, R. (eds.) CVRMed/MRCAS -1997. LNCS, vol. 1205, pp. 213–222. Springer, Heidelberg (1997). doi:10.1007/BFb0029240
39. Canny, J.: A computational approach to edge detection. IEEE Trans. Pattern Anal. Mach. Intell. **6**, 679–698 (1986)
40. Leung, T., Malik, J.: Representing and recognizing the visual appearance of materials using three-dimensional textons. IEEE Trans. Med. Imaging **43**, 29–44 (2001)
41. Schmid, C.: Constructing models for content-based image retrieval. In: Proceedings of the 2001 IEEE Computer Society Conference on Computer Vision and Pattern Recognition, CVPR 2001, vol. 2, pp. II-39. IEEE (2001)
42. Li, C., Xu, C., Gui, C., Fox, M.D.: Distance regularized level set evolution and its application to image segmentation. IEEE Trans. Med. Imaging **19**, 3243–3254 (2010)
43. Web, B.: Simulated brain database. McConnell Brain Imaging Centre, Montreal Neurological Institute, McGill (2004). http://www.bic.mni.mcgill.ca/brainweb/
44. Chan, T.F., Vese, L., et al.: Active contours without edges. IEEE Trans. Med. Imaging **10**, 266–277 (2001)
45. Wells, W.M., Grimson, W.E.L., Kikinis, R., Jolesz, F.A.: Adaptive segmentation of MRI data. IEEE Trans. Med. Imaging **15**, 429–442 (1996)